crystals

MDPI

Article

Unveiling the Mechanisms of High-Temperature 1/2[111] Screw Dislocation Glide in Iron–Carbon Alloys

Ivaylo Hristov Katzarov [1,2,*] and Ljudmil Borisov Drenchev [1]

[1] Institute of Metal Science, Equipment and Technologies with Hydro- and Aerodynamics Centre, Bulgarian Academy of Sciences, 67 Shipchenski Prohod Str., 1574 Sofia, Bulgaria; ljudmil.d@ims.bas.bg
[2] Department of Physics, King's College London, Strand, London WC2R 2LS, UK
* Correspondence: ivaylo.katsarov@kcl.ac.uk

Abstract: We have developed a self-consistent model for predicting the velocity of 1/2[111] screw dislocation in binary iron–carbon alloys gliding by a high-temperature Peierls mechanism. The methodology of modelling includes: (i) Kinetic Monte-Carlo (kMC) simulation of carbon segregation in the dislocation core and determination the total carbon occupancy of the core binding sites; (ii) Determination of kink-pair formation enthalpy of a screw dislocation in iron—carbon alloy; (iii) KMC simulation of carbon drag and determination of maximal dislocation velocity at which the atmosphere of carbon atoms can follow a moving screw dislocation; (iv) Self consistent calculation of the average velocity of screw dislocation in binary iron–carbon alloys gliding by a high-temperature kink-pair mechanism under a constant strain rate. We conduct a quantitative analysis of the conditions of stress and temperature at which screw dislocation glide in iron–carbon alloy is accomplished by a high-temperature kink-pair mechanism. We estimate the dislocation velocity at which the screw dislocation breaks away from the carbon cloud and thermally-activated smooth dislocation propagation is interrupted by sporadic bursts of dislocation activity.

Keywords: dislocations; diffusion; FeC alloy; dynamic strain aging

check for updates

Citation: Katzarov, I.H.; Drenchev, L.B. Unveiling the Mechanisms of High-Temperature 1/2[111] Screw Dislocation Glide in Iron–Carbon Alloys. *Crystals* **2022**, *12*, 518. https://doi.org/10.3390/cryst12040518

Academic Editor: Wojciech Polkowski

Received: 19 March 2022
Accepted: 5 April 2022
Published: 8 April 2022

Publisher's Note: MDPI stays neutral with regard to jurisdictional claims in published maps and institutional affiliations.

Copyright: © 2022 by the authors. Licensee MDPI, Basel, Switzerland. This article is an open access article distributed under the terms and conditions of the Creative Commons Attribution (CC BY) license (https://creativecommons.org/licenses/by/4.0/).

1. Introduction

Steel plasticity is strongly influenced by interactions between solute atoms, such as carbon, and dislocations [1]. It is commonly accepted that the segregation of solute atoms in the surroundings of dislocations, forming clouds of impurities known as Cottrell atmospheres, is the underlying atomistic mechanism behind steel hardening [2–4]. The atmosphere is known to pin dislocations and render them less mobile. As more carbon atoms segregate, the atmosphere grows around the dislocations and hinders dislocation motion. Higher stresses are then required to unpin the dislocation from the solutes. The hardening of a material that is aged for a certain period of time after undergoing plastic deformation is defined as static strain aging. In contrast to static strain aging, which occurs during the specimen rest time, another strain aging phenomenon, called dynamic strain aging takes place during the plastic deformation of a specimen. It is associated with the diffusion of impurities to a mobile dislocation temporarily arrested at obstacles.

Carbon-induced strengthening of bcc iron has been studied in [5] using molecular dynamics (MD) simulations and a stohastic model based on minimum-energy path calculations and transition state theory. Plastic deformation of a solid solution where dislocations pass a random distribution of atomic-size obstacles have been studied by MD simulations in [6]. Simulations of a single edge dislocation in Ni-Al alloy reveal that dislocations propagate through jerky avalanches, the size and duration of which are power-law distributed. Dislocation propagation above the depinning threshold has been characterized by the distributions of avalanche area and duration. The analysis of atomic-scale dislocation dynamics has revealed a number of signatures of criticality. Microscopic mechanisms of DSA

in W-O interstitial solid solutions has been studied at atomic scale [7]. Simulations have been performed using a kinetic Monte Carlo model that accounts for kink-pair nucleation and solute diffusion. Solute cloud formation, solid solution strengthening and dislocation/solute coevolution leading to jerky flow have been revealed from the simulations. A kMC model of screw dislocation glide and solute diffusion in substitutional W-Re alloy has been developed in [8]. The model has been applied for studying the mechanisms governing dislocation kinetics. The intrinsic drawback of both MD and kMC simulations of dislocation/solute coevolution is that diffusion and kink-pair nucleation are rare events operating on different timescales.

Recent measurements by Caillard [9] in binary iron–carbon alloys with carbon concentrations of 1, 16 and 230 atomic parts per million (appm), reveal that the dynamic interaction between mobile dislocations and solute carbon atoms results in dynamic strain aging effects in the temperature range of 100–300 °C. Caillard found three regimes of behaviour: (i) the expected Peierls mechanism of kink pair formation and migration at low temperature; (ii) at intermediate temperatures carbon atoms become sufficiently mobile to reach and segregate in the core of nearest dislocation and immobialize it. Dislocations start to move in bursts—no dislocation motion is observed upon straining before a source is unlocked and emits many dislocations. This results in the dynamic strain aging effect characterized by avalanches of rapid dislocation glide corresponding to the observed jerky and serrated flow. (iii) Above about 200 °C, a new mechanism was discovered, namely viscous glide accomplished by a Peierls mechanism but with an activation energy almost twice that of the room temperature viscous flow. The transitions between these domains vary as a function of dislocation velocity, but so far a quantitative analysis and confirmation of observation with theory and modelling has been lacking.

A dislocation drag mechanism, by which dislocations can collect and transport carbon within their cores, takes place if the diffusion of carbon atoms and the motion of dislocations occur with rates in the same order of magnitude. It can be assumed that dislocations glide is accomplished by a high-temperature Peierls mechanism when carbon atoms in bcc-iron become mobile enough to follow gliding dislocations. To study the drag of carbon atoms by dislocations requires simulation techniques that capture carbon diffusion events, trapping and escaping from the core and the motion of dislocations simultaneously. Caillard [9] ascertained that dynamical strain aging is caused by the trapping of carbon by straight screw segments of $1/2[111]$ dislocations. For this reason we focus on the $1/2[111]$ screw dislocation in the present work. In [10] we have developed an atomistic kinetic Monte-Carlo (kMC) model describing carbon diffusion in the non-homogeneous stress field created by a $1/2[111]$ screw dislocation in bcc-iron, where the behaviour of individual atoms is explicitly taken into account. The kMC model employs information gathered from molecular statics simulations carried out in order to determine the activation energies required for carbon hops in the neighbourhood of the line defect [11]. The number of segregated carbon atoms forming a Cottrell atmosphere around a $1/2[111]$ screw dislocation, predicted by performing long time kMC simulations, has been validated against the carbon atmosphere visually identified by position-sensitive atom probe microscopy [12]. The kMC model allows us to study both the diffusing carbon residing in the dislocation core, and carbon atoms which move through the interstitial sites in dislocation surroundings. We have employed the kMC model to simulate carbon diffusion in bcc–iron leading to the formation of Cottrell atmosphere. The kMC approach also offers an atomistic view of the carbon drag mechanism. By setting the dislocation to glide with constant velocity v_{dis}, we can simulate the evolution of the carbon cloud around the moving linear effect. This approach allows us to estimate the maximal dislocation velocity $v_{\max}(T, C)$ at which the atmosphere of carbon atoms can follow a moving screw dislocation. When dislocation velocity is higher than $v_{\max}$, dislocations gradually break away from the carbon clouds. Carbon atoms trapped in the core can follow the dislocation if it glides slowly and viscously via a Peierls mechanism (the process of kink pair creation followed by kink migration). However, we do not consider kink pair formation and migration explicitly

in the kMC model. We therefore turn now to the problem of predicting v_{dis} within the Peierls mechanism. v_{dis} is then the dislocation velocity averaged over the numerous acts of kink-pair creation and migration processes. The trapped C atoms strongly modify the kink pair formation enthalpy E_{kp}, which for a given resolved shear stress is a function of the solute concentration and the rate at which impurities are distributed among trap sites [13]. At lower solute atom mobility, the impurities remain behind in binding sites of higher potential energy as a dislocation segment moves between Peierls valleys, leading to a higher Peierls barrier and E_{kp}. The Peierls barrier becomes smaller as the rate at which solute atoms are distributed among the trap sites increases [13]. With increasing temperature, the number of solute atoms trapped in the core decreases, which also reduces the Peierls barrier [14]. Hence, as temperature increases, E_{kp} decreases as a consequence of the decreasing Peierls barrier. It could be expected that a screw dislocation can glide via a high-temperature Peierls mechanism if: (a) the kink-pair formation energy barrier, E_{kp}, becomes smaller as the mobility of carbon atoms trapped in the dislocation core increases at high temperature; (b) the carbon Cottrell atmosphere can follow the dislocation, that is, a dislocation's average velocity at a given carbon concentration and temperature is lower than $v_{\max}$. The transitions to high-temperature viscous glide accomplished by a Peierls mechanism vary as a function of dislocation velocity. The problem of predicting v_{dis} within the Peierls mechanism is related to predicting kink-pair formation enthalpy E_{kp} at a given carbon concentration and local shear stress τ. Here, we present a self consistent model that is able to predict the average velocity of screw dislocation in binary iron–carbon alloys gliding by a high-temperature kink-pair mechanism. The purpose of the present work is conducting a quantitative analysis of the conditions of stress and temperature at which a screw dislocation glide is accomplished by a high-temperature kink-pair mechanism and transition may occur between carbon drag and breakaway. We aim to understand whether the dislocation behaviour in the high temperature domain of DSA described in [9] is related to the occurrence of the "high-temperature Peierls mechanism". The structure of the paper is as follows. Section 2 presents our methodology of modelling: in Section 2.1, we examine the effect of trapped carbon on the motion of a straight dislocation between two adjacent Peierls valleys. Section 2.2 addresses the effect of carbon segregated in the dislocation core on kink-pair formation. In Section 2.3, we present a self consistent model for the determination of the average velocity of screw dislocation in binary iron–carbon alloys gliding by a high-temperature kink-pair mechanism under a constant strain rate. Sections 3 and 4 are our results and discussion sections. We conclude in Section 4.

2. Materials and Methods

2.1. Carbon Effect on the Dynamics of Straight Dislocation

Density functional theory (DFT) calculations have identified two core structures of the 1/2[111] screw dislocation in bcc Fe. The so called "easy core" (EC) is the stable configuration, and the metastable "hard core" (HC), which is very close in configuration to the "saddle point" core [15,16]. Tight-binding (TB) simulations of carbon interactions with the 1/2[111] screw dislocation found solute distribution to vary significantly between the easy and hard cores [17]. The binding sites of carbon, and their strengths, were determined by the TB calculations of carbon–screw dislocation interactions. These were performed using the Fe-C TB model of Paxton and Elsässer [18]. The binding energies of carbon to both the hard and easy cores, with the resulting distribution of carbon can be seen in Figure 1.

These binding energies agree well with experiments and atomistic/elastic calculations [16,19]. In agreement with DFT, the highest binding energy is found in the centre of the hard screw core [19]. As a dislocation moves from EC to HC to EC, the trap sites ahead of the dislocation line transform into HC sites before finally transforming into EC trap sites behind the dislocation line. These atomistic results provide data for determination of kink-pair formation energies as a function of stress and carbon concentration, C, using a line tension (LT) model of a screw dislocation [15]. A segment of a streight dislocation

lying in its Peierls valley has to migrate towards or into the next Peierls valley so as to make an incipient or complete kink pair. Within the LT model, the dislocation is divided into segments of width b, the Burgers vector, along its length. The energy per unit length of dislocation is then described by the following line tension expression [15].

$$E = \sum_j E_j = \frac{1}{2}K\sum_j (x_j - x_{j+1})^2 + \sum_j E_P(x_j) - \sum_j \varepsilon_{1pq}\tau_{pr}b_r\xi_p x_j - \sum_k E_k^c(|x_j - x_C|) \quad (1)$$

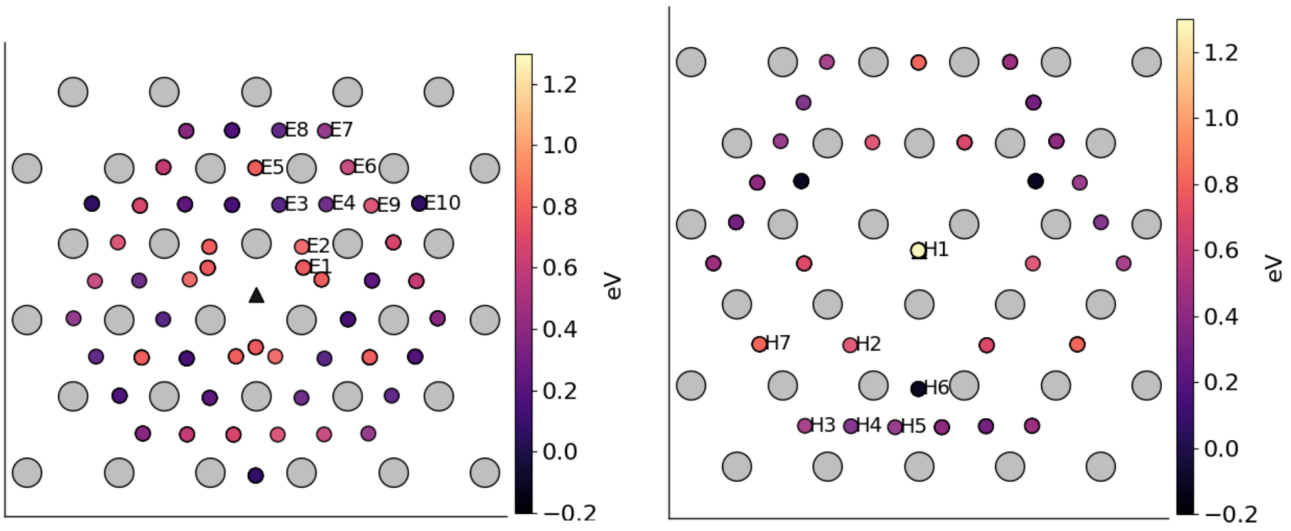

(**a**) (**b**)

Figure 1. The binding sites and binding energies of carbon segregated around: (**a**) easy 1/2[111] screw dislocation core; (**b**) hard 1/2[111] screw dislocation core.

The variable x_j describes the deviation of the jth segment from the dislocation's original position in the Peierls valley. The first term describes the energy penalty for two segments which have different amounts of deviation from the original Peierls valley towards the next and K is the associated "spring constant". The periodic Peierls energy landscape is described by an energy function, $E_P(x_j)$. The third term is the component perpendicular to the line sense ξ of the Peach–Kohler force arising from a local stress **ø** times the displacement of the jth segment. ε_{1pq} is the Levi–Civita symbol where 1-component is perpendicular to [111] direction. The final term expresses the energy associated with carbon atoms that are trapped at the binding sites in the dislocation core at a distance $|x_j - x_C|$ from the core, in which x_C is the position of the kth carbon atom relative to the elastic centre. Here, $0 < x < h$, where h is the period of the Peierls potential on the (110) plane. This term varies when a dislocation segment propagates between two adjacent Peierls valleys as a result of the variation in the binding energies $E_k^c(x)$ and carbon redistribution between trap sites. We parameterise $E_k^c(x)$ by fitting and interpolation of tigth-binding data [17]. We define

$$\chi_t = \sum_i \chi_i = const \quad (2)$$

as the total carbon occupancy of the core sites. We assume that χ_t is constant, that is, carbon will redistribute dynamically between trap sites during dislocation propagation between two Peierls valleys, but overall the dislocation will not absorb or reject carbon. We also only allow C to redistribute among traps within a plane perpendicular to the dislocation line,

in view of the slower carbon pipe diffusivity [10]. We define the equilibrium occupation probability, χ_i^e of trap site i as [20],

$$\chi_i^e(x) = \frac{\chi_i e^{-E_i^c(x)/kT}}{\sum_j \chi_j e^{-E_j^c(x)/kT}} \tag{3}$$

Within the line tension model (1), we have a complete description of the energetics of the dislocation as a function of x and χ_t only in two limiting cases: (a) slow glide, in which traps are occupied according to (3), and (b) fast glide, in which all carbon atoms are fixed in the traps they occupy in the initial state before glide. Figure 2 shows potential energy profiles in both limiting cases for carbon concentration in the bulk C = 250 appm.

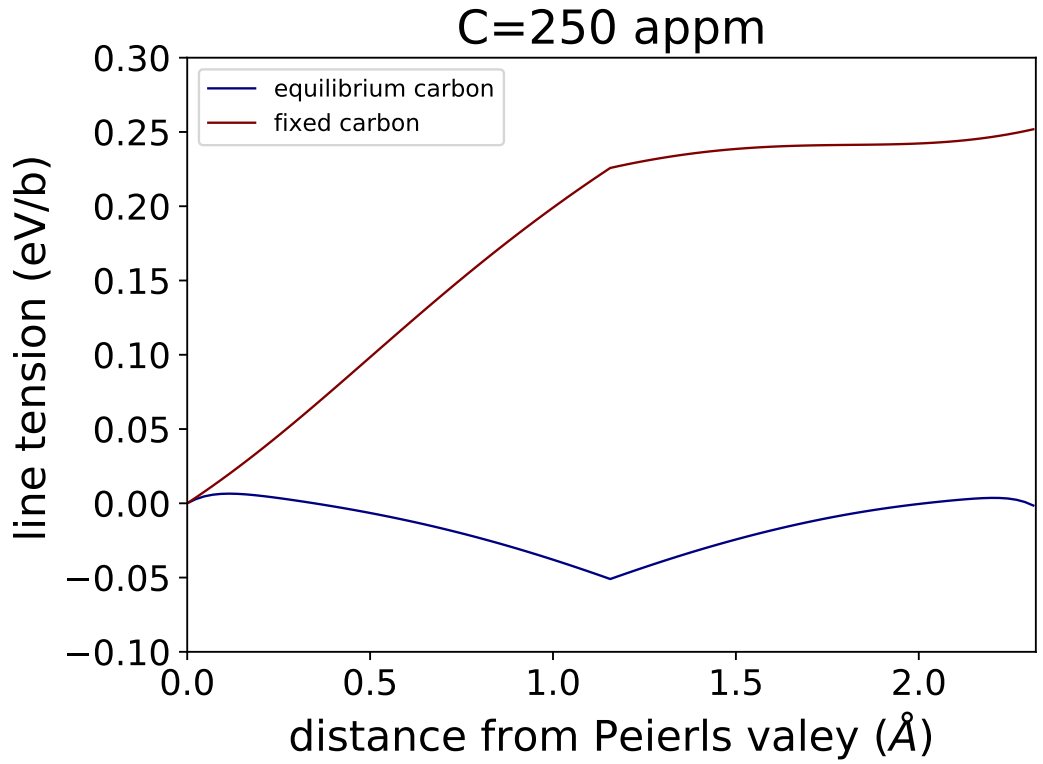

Figure 2. Potential energy of a straight 1/2[111] screw dislocation.

In the equilibrium limit, the effect of carbon trapped in deeper traps is strong enough that for carbon concentration in the bulk, C = 250 appm, the hard core is lower in energy than the easy core, and their roles are reversed. This result agrees well with DFT simulations by Ventelon [19]. When a carbon is placed in the vicinity of a relaxed easy dislocation core, a spontaneous reconstruction of the dislocation core occurs: from easy to hard. In the limit of rapid glide, carbon remains behind in sites of higher binding energy, leading to higher Peierls barrier. The actual dislocation energy profile between two Peierls valleys will be controlled by the dislocation velocity, v. Therefore, we need a theory that will predict the energy profile as a function of v. We may assume that the difference between the probability of the occupancy of trap i, $\chi_i(x)$, and its equilibrium value (3), $\chi_i^e(x)$ is the driving force for carbon redistribution between trap sites. For any of the binding sites, we find the following continuity equation,

$$\frac{\partial \chi_i(x,v)}{\partial t} = v\frac{\partial \chi_i(x,v)}{\partial x} = -\sum_{i \neq j}(\chi_i(x,v) - \chi_i^e(x))R \tag{4}$$

where $R = fexp(-E_i(x)/kT)\left(\chi_j^e(x) - \chi_j(x,v)\right)$ if $\left(\chi_i > \chi_i^e\right)$ and $\left(\chi_j < \chi_j^e\right)$; $R = fexp(-E_j(x)/kT)\left(\chi_j(x,v) - \chi_j^e(x)\right)$ if $\left(\chi_i < \chi_i^e\right)$ and $\left(\chi_j > \chi_j^e\right)$; f is an "attempt frequency" for carbon to escape from the ith trap. By solving (4), subject to the condition (2), we may determine the potential energy of the dislocation as a function of position between two Peierls valleys and velocity v.

2.2. Kink Pair Formation Enthalpy

Formation of a kink pair is a result of numerous random events in which a small segment of dislocation moves towards a neighbouring Peierls valley producing an "incipient" kink pair. The elastic attraction of the kinks leads to the annihilation of most of the "incipient" kink pairs. The formation of a stable kink pair is a result of increasing distance between kinks under the action of the applied shear stress. We do not consider these processes explicitly in our simulations. Trapped carbon strongly modifies the kink-pair formation energy, E_{kp}. E_{kp} is a function of v_{dis} since the distribution of carbon among binding sites will depend on how fast the dislocation is moving. Using the LT model, the energy, $E_j(C, x, v_{dis})$, of a dislocation segment of length b between two Peierls valleys, can be calculated. Then, using the "nudged elastic band" (NEB) method [21], we may calculate the kink pair activation energy, $E_{kp}(C, \tau, v_{dis})$ [14,15] for a given resolved shear stress, τ, and an assumed v_{dis}. However, dislocation velocity v_{dis} is a function of E_{kp}. We assume that v_{dis} is constant, and

$$v_{dis}(E_{kp}) = \frac{h}{t_r} \tag{5}$$

where we define an average relaxation time for kink-pair formation,

$$t_r = f_{kp}^{-1} e^{E_{kp}(C,\tau,v)/kT} \tag{6}$$

The frequency prefactor f_{kp} has been determined by comparing the velocity of a pure screw segment in bcc-Fe calculated from the kMC model of 1/2[111] screw dislocation with the experimentally estimated velocity [14]. We find $f_{kp} = 2.31 \times 10^9$ s^{-1}.

To find a self consistent solution of (5) and (6), and to determine E_{kp} at a given C and τ, we proceed with the following iterative process.

1. Assume an initial E_{kp}.
2. Calculate the corresponding v_{dis} using (5) and (6).
3. Determine the distribution of carbon from the continuity Equation (4), subject to (2); and calculate the segment energy, $E_j(C, x, v_{dis})$ from the LT model.
4. Calculate E_{kp} using the NEB and go to step 2.

This process is iterated until the E_{kp} calculated in step 4 is no longer changing to within some tolerance.

2.3. Self-Consistent Calculation of Dislocation Velocity in Binary Iron–Carbon Alloys

The velocity of a screw dislocation, steadily moving by the kink-pair mechanism, can be expressed as

$$v_{dis} = f_{kp} \frac{hL}{w} e^{-E_{kp}(\tau,C)/kT} \tag{7}$$

where w is the critical width of a stable kink pair and L is the dislocation length. Molecular dynamics simulations have identified the critical width of the 1/2 [111] screw dislocation as $w \approx 30b$ [22]. The increased probability of kink pair formation on all three [110] glide planes leads to an increased likelihood of kink pair collisions resulting in the formation of cross-kinks [13,14]. Equation (7) does not take into account the effects of cross-kink formation and self pinning on the dislocation mobility. In order to emulate experimental tests, which are performed under a constant strain rate, $\dot{\varepsilon}_0$, and temperature, T, we carry

out strain rate-controlled simulations. The instantaneous shear stress resulting from a given $\dot{\varepsilon}_0$ is obtained as:

$$\tau(t) = 2\mu[t\dot{\varepsilon}_0 - \varepsilon_p(t)] \quad (8)$$

where ε_p is the total accumulated plastic strain and μ is the shear modulus

$$\varepsilon_p(t^{n+1}) = \varepsilon_p(t^n) + \delta\varepsilon_p(t^{n+1}) \quad (9)$$

t is the total simulation time and δt^{n+1} is the current timestep. The plastic strain update is obtained from the dislocation velocities calculated at each stress using Orowan's equation, as:

$$\delta\varepsilon_p(t^{n+1}) = \rho_d b v_{dis}(\tau)\delta t^{n+1} \quad (10)$$

where $v_{dis}(\tau)$ is the dislocation velocity, which depends on the resolved shear stress τ and carbon atoms trapped in the dislocation core; ρ_d is dislocation density. In order to determine self-consistently the velocity of screw dislocation in binary iron–carbon alloys gliding by a high-temperature Peierls mechanism, we proceed with the following iterative process.

1. Calculate the v_{dis} at the initial shear stress τ using (7) and determined by $E_{kp}(\tau, C)$.
2. From the dislocation velocity calculated at stress τ, we calculate the total accumulated plastic strain from (9) and (10).
3. The instantaneous shear stress τ resulting from the calculated accumulated plastic strain is obtained from (8).
4. Go to step 1

If dislocation breaks away from the carbon cloud, the steady dislocation propagation by the Peierls mechanism is replaced by a thermally-activated screw dislocation burst in carbon-free regions with a lower kink-pair formation energy interrupted by interactions with solute atoms. In the carbon-free regions, the kink-pair activation energy $E_{kp}(\tau, C)$ in (7) is replaced by the corresponding kink-pair formation enthalpy in bcc-Fe.

3. Results

The kMC treatment of carbon Cottrell atmosphere formation presented in this work considers a portion of the atmosphere contained inside a fixed volume parallelepipedal region $10 \times 10 \times 10$ nm^3, the rectangular cross section of which (10×10 nm^2) corresponds approximately to the surrounding dislocation core region of the atom probe experiments [12].

In the present study, the surroundings of the dislocation core (region with radius $R \approx 0.6$ nm in the direct neighbourhood of the dislocation centre [11]) are connected to an infinite carbon reservoir, such that no carbon depletion occurs in the matrix due to segregation [10]. The evolution of the number of carbon atoms segregated to form an atmosphere around a 1/2[111] screw dislocation at a background carbon concentration of 250 appm simulated by our kMC model is shown in Figure 3.

The kMC calculations allow us to predict the rate of formation and strength of carbon atmospheres.

The simulations show that at $T = 400$ K, an equilibrium carbon Cottrell atmosphere is formed after 100 s. At 500 K, the equilibrium carbon Cottrell atmosphere around a screw dislocation is formed even faster—0.3 s for 250 appm. At equilibrium, the average number of carbon atoms trapped in the screw dislocation core is around 5 C/nm at 400 K and 2.3 C/nm at 500 K.

From these kMC simulations, we determine the total carbon occupancy of the core binding sites χ_t.

The kMC treatment of the carbon drag mechanism presented in this section considers the evolution of the carbon cloud dragged by a mobile straight screw dislocation inside a fixed volume parallelepipedal region $60 \times 10 \times 10$ nm^3. At the starting time $t = 0$, the carbon atoms segregated to form an atmosphere around the 1/2[111] screw dislocation are at equilibrium with the background carbon concentration. We employ the kMC model to simulate the redistribution of carbon atoms when dislocation migrates in the (110) glide plane with constant velocity v_{dis} (Figure 4).

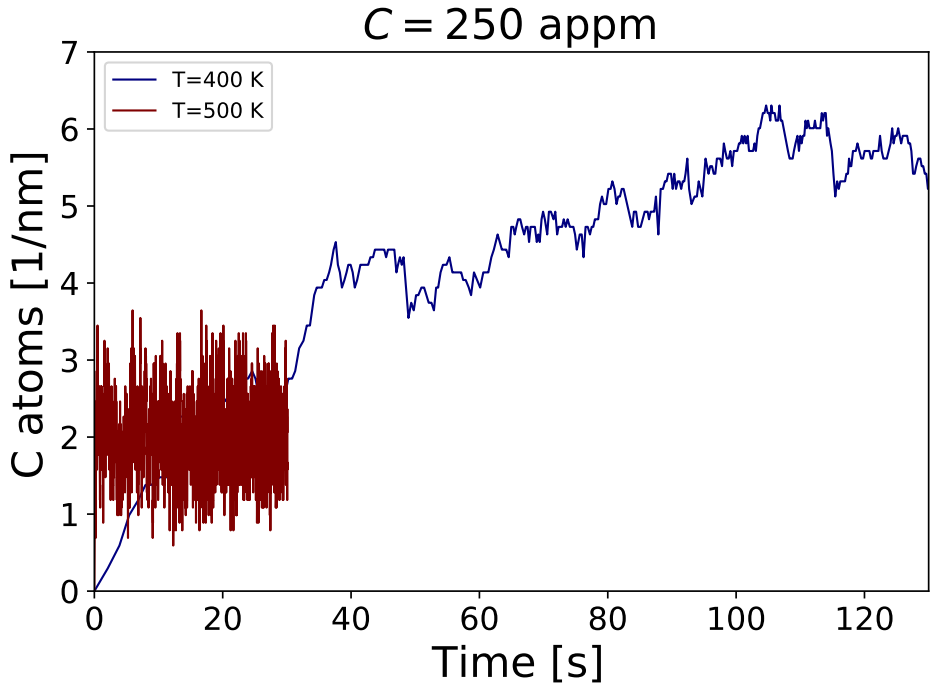

Figure 3. The number of carbon atoms per 1 nm trapped in the dislocation core at two different temperatures.

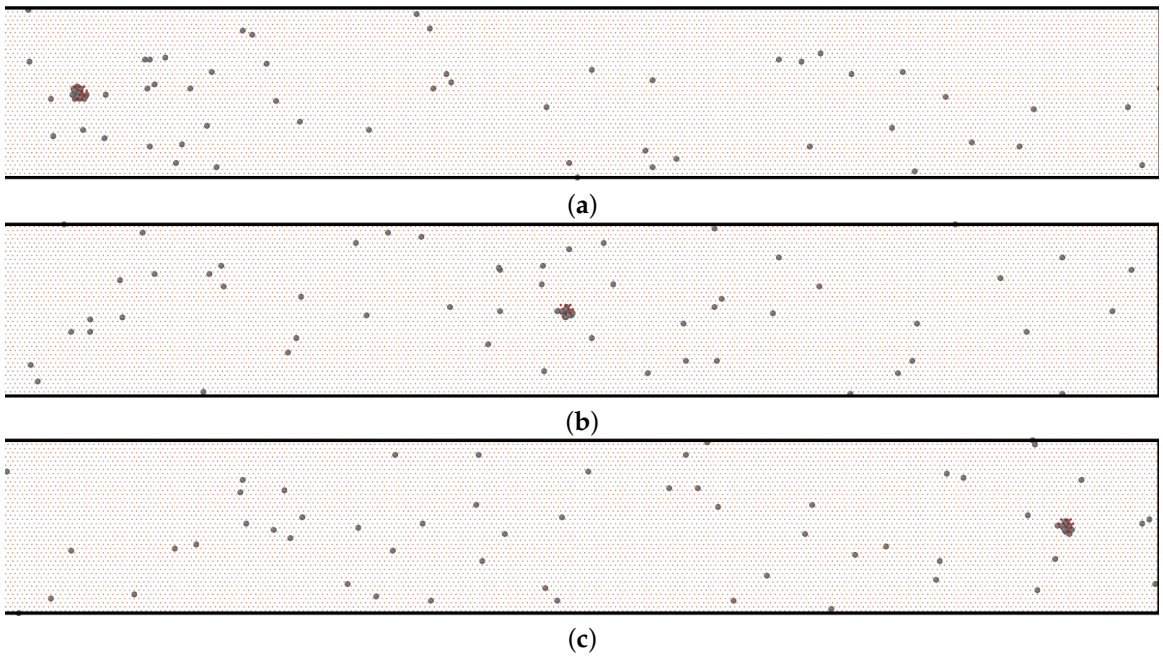

Figure 4. The motion of a screw dislocation dragging carbon, illustrated by a series of snapshots. KMC simulations are carried out at dislocation velocity $v_{dis} = 0.1$ nm/s and temperature 400 K; (**a**) t = 0 s; (**b**) t = 25 s; (**c**) t = 52 s.

The number of carbon atoms effectively dragged by the dislocation as a function of the dislocation travel distance is shown in Figure 5 for different dislocation velocities and temperatures of 400 K and 500 K. From the above simulations, we evaluate the maximal dislocation velocity $v_{\max}$ at which the atmosphere of carbon atoms can follow a moving screw dislocation (Figure 6).

Figure 7 shows the results of the self-consistent iterative procedure for the calculation of kink-pair formation enthalpy E_{kp} proposed in Section 2.2.

We may interpret Figure 7 in the following way. At high stress, E_{kp} is smaller because the process of dislocation segment transition to the adjacent Peierls valley is dominated by the applied stress.

At low stress, we observe a large E_{kp}, the largest being that of zero stress. As temperature increases, E_{kp} decreases as a consequence of the decreasing Peierls barrier resulting from the enhanced carbon mobility and lower C occupancy in the core. After determination of E_{kp} as a function of τ and C, we apply the self-consistent procedure described in Section 2.3 to determine the evolution of the 1/2[111] screw dislocation velocity during a strain rate-controlled simulation of dislocation motion in binary iron–carbon alloys. Dislocation density in our simulations is $\rho_d = 10^{13}$ m^{-2}. ρ_d sets the dislocation line length to a magnitude of approximately $L = (\rho_d)^{-1/2}$, which for $\rho_d = 10^{13}$ m^{-2}, gives $L = 1280b$. The simulations are performed under a constant strain rate, $\dot{\varepsilon}_0 = 10$ s^{-1}. Evolution of the velocity and stress with time during a strain rate-controlled simulation of dislocation motion at T = 400 K and T = 500 K are shown respectively in Figures 8 and 9.

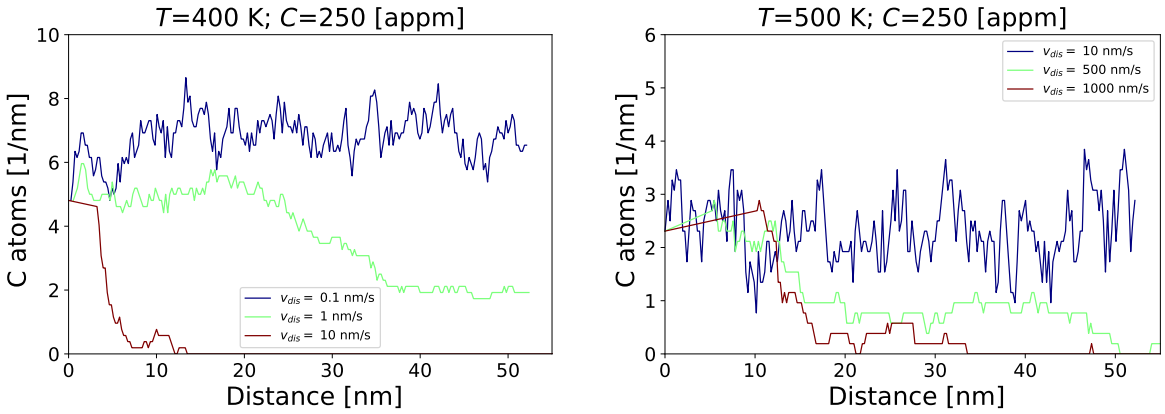

(**a**) (**b**)

Figure 5. The evolution of the number of carbon atoms per 1 nm trapped in the core of a moving straight dislocation as a function of the travel distance; (**a**) T = 400 K; (**b**) T = 500 K.

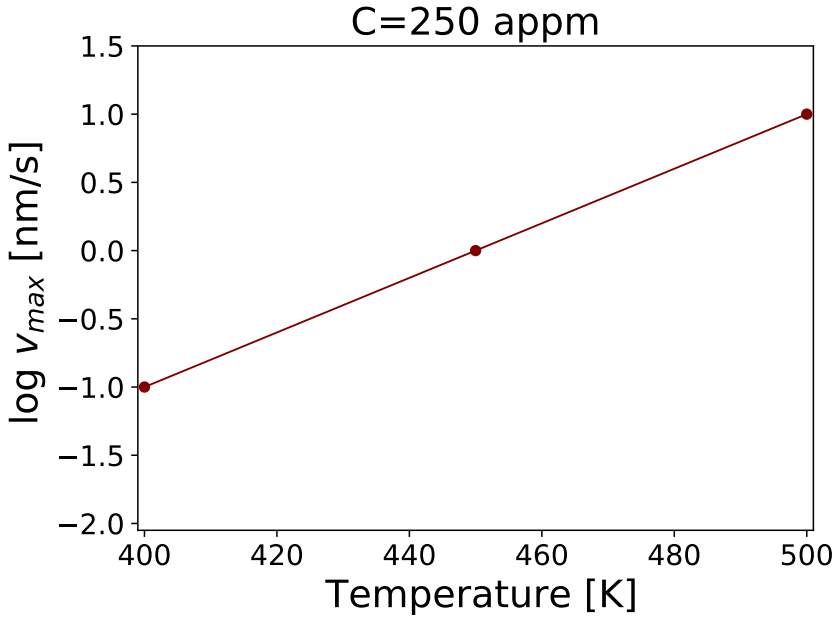

Figure 6. The maximal dislocation velocity $v_{\max}$ at which the atmosphere of carbon atoms can follow a moving screw dislocation at different temperatures.

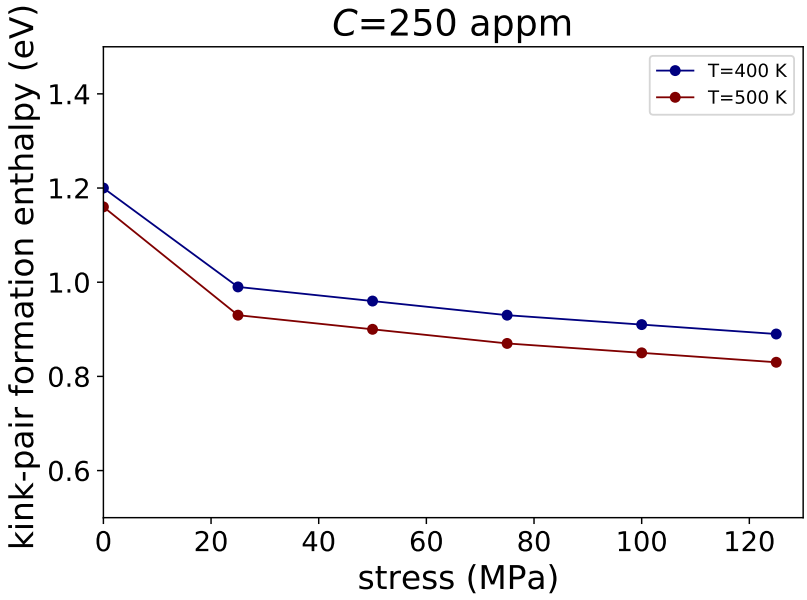

Figure 7. Kink pair formation enthalpy, E_{kp}, as a function of resolved shear stress, calculated by iterative solution of Equations (5) and (6).

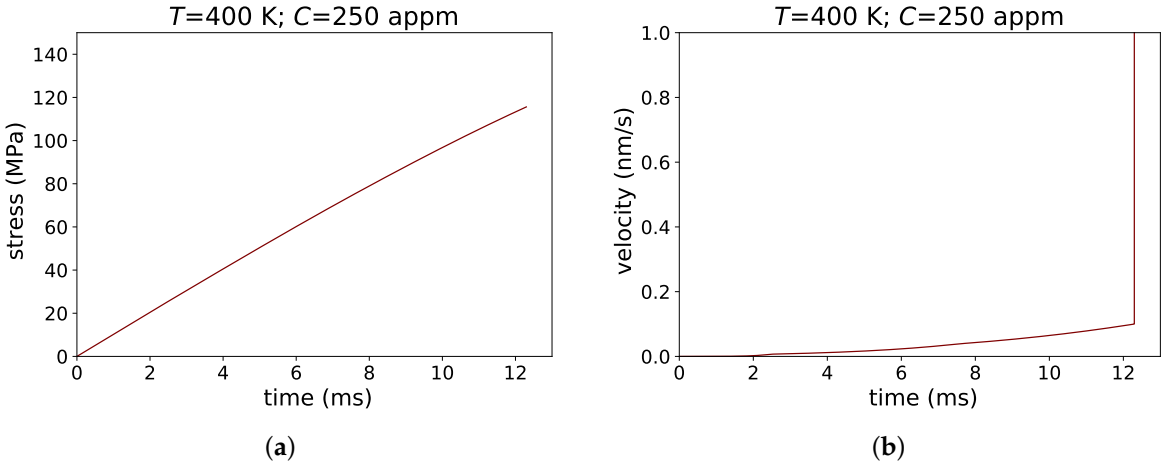

(**a**) (**b**)

Figure 8. Evolution of the stress and dislocation velocity with time during simulation of dislocation motion at T = 400 K; (**a**) stress; (**b**) velocity.

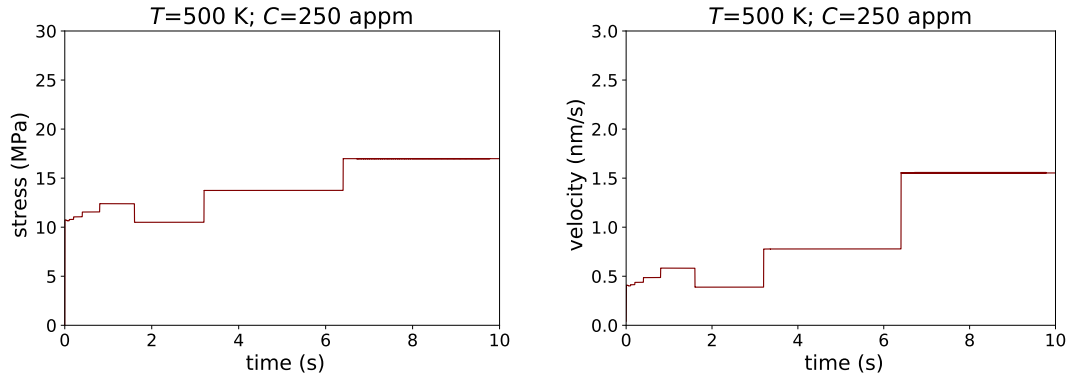

(**a**) (**b**)

Figure 9. Evolution of the stress and dislocation velocity with time during simulation of dislocation motion at T = 500 K; (**a**) stress; (**b**) velocity.

4. Discussion

We use our approach to simulate screw dislocation propagation by kink-pair mechanism in an iron–carbon system at two temperatures—400 K and 500 K, which belong to two regimes of behaviour found by Caillard [9] (intermediate temperatures where dislocations start to move in bursts and high-temperatures above about 200 °C where dislocations move slowly and steadily by a possible Peierls mechanism). The experiments [9] show that the temperatures at which the screws move slowly, presumably by high-temperature kink-pair mechanism, are almost independent of the carbon concentration.

At 400 K, carbon atoms become sufficiently mobile to move to the nearest dislocations and hinder dislocation motion. The trapped solute atoms remain behind in binding sites of higher potential energy as a dislocation segment moves, leading to a higher Peierls barrier and kink-pair formation energy E_{kp} (Figure 7). Higher stresses are then required to increase kink-pair formation rate and dislocation velocity. The carbon atoms have sufficient time to follow the dislocation at lower dislocation velocities (Figure 5a). kMC simulations reveal that at 400 K and at background carbon concentrations of 250 appm, the maximal dislocation velocity $v_{\max}$ at which the atmosphere of carbon atoms can follow a moving screw dislocation is 0.1 nm/s. The accumulated plastic strain induced by dislocations gliding at low velocities $v_{dis} < v_{\max}$ can not efficiently relieve the shear stress resulting from the constant shear strain rate (Figure 8a). The rising shear stress increases the velocity of dislocation gliding by kink-pair mechanism. When v_{dis} exceeds $v_{\max}$, dislocations break away from the carbon clouds and start to move in carbon-free regions with a lower kink-pair formation energy interrupted by interactions with solute atoms. Plastic deformation of a solid solution where dislocations pass a random distribution of atomic-size obstacles have been studied in [6]. MD simulations of a single edge dislocation in a binary alloy reveal that dislocations propagate through jerky avalanches. In this work, we do not simulate dislocation motion after dislocation breaks away from the carbon cloud. We only consider the initial acceleration of dislocations in the carbon-free region. In the carbon-free region, we calculate the dislocation velocity using Equation (7), where the kink-pair activation energy $E_{kp}(\tau, C)$ is replaced by the corresponding kink-pair nucleation enthalpy $E_{kp}(\tau)$ in bcc-Fe which, for applied shear stress $\tau = 115$ MPa (Figure 8a), is $E_{kp}(\tau) = 0.35$ eV [15]. Due to the lower kink-pair formation energy in bcc-Fe, after breaking away from the carbon cloud, the dislocation accelerates to a velocity which is six orders of magnitude higher then $v_{\max}$. The abrupt increase in the dislocation velocity relieves the stress, which results in decreasing v_{dis} below $v_{\max}$. After restoration of the kink-pair, the glide dislocation velocity gradually increases above $v_{\max}$, leading to repeated bursts of rapid dislocation glide. The studied thermally-activated smooth dislocation propagation is interrupted by abrupt sporadic bursts of screw dislocation activity.

At higher temperatures, the number of carbon atoms trapped in the core decreases, which reduces the barrier between two adjacent Peierls valleys. The Peierls barrier is additionally reduced as the rate at which carbon atoms are distributed among trap sites increases. Hence, as the temperature increases, the kink-pair formation enthalpy E_{kp} decreases as a consequence of the decreasing Peierls barrier (Figure 7). At higher temperatures, carbon has a sufficiently high mobility to keep up with faster dislocations (Figure 5b). Due to the higher $v_{\max}$ and lower E_{kp}, the accumulated plastic strain, induced by dislocations gliding by kink-pair mechanism, relieves the shear stress, resulting in relatively long periods of steady dislocation glide by kink-pair mechanism (Figure 9b). The periods of steady propagation are interrupted by more abrupt changes in stress and velocity due to the interactions between carbon and dislocations (Figure 9). The average dislocation velocity determined in the present simulation is 0.93 nm/s. The average velocity depends on the loading conditions. Figure 10 shows the evolution of the velocity with time during a strain rate-controlled simulation of dislocation motion for three different strain rates $\dot{\varepsilon}_0$. With an increase in the constant strain rate, the average dislocation velocities increase, and for $\dot{\varepsilon}_0$, shown in Figure 10, they are correspondingly 0.1 nm/s, 0.42 nm/s and 1.3 nm/s. The experimentally observed average dislocation velocity at C = 230 appm and T = 200 °C reported

in [9] is 0.27 nm/s. Formation of cross-kinks resulting from kink collisions amount to self pinning points which reduce dislocation mobility. The present model does not take into account the effects of cross-kinks formation and self pinning on the dislocation mobility.

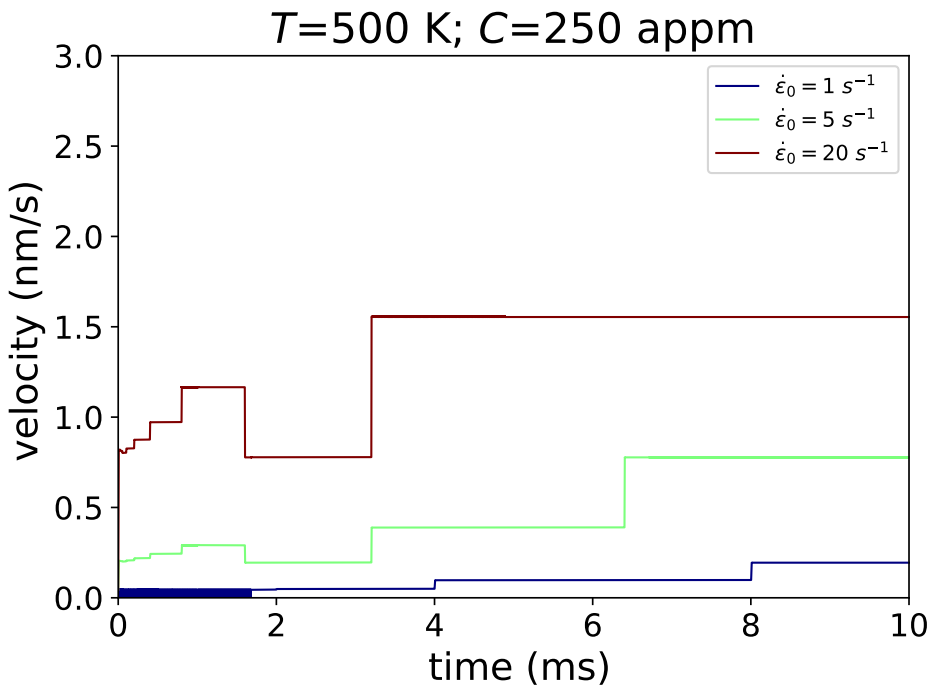

Figure 10. Evolution of the dislocation velocity with time during the simulation of dislocation motion at T = 500 K for three constant strain rates.

5. Conclusions

We have developed a self-consistent model for predicting the velocity of 1/2[111] screw dislocation in binary iron–carbon alloys gliding by a high-temperature Peierls mechanism. The methodology of modelling includes:

- KMC simulation of carbon segregation in dislocation core and determination the total carbon occupancy of the core binding sites.
- Evaluation of the effect of trapped carbon on the motion of a straight dislocation segment between two adjacent Peierls valleys.
- Determination of kink-pair formation enthalpy E_{kp} of a screw dislocation in iron—carbon alloy.
- KMC simulation of carbon drag and determination of maximal dislocation velocity $v_{\max}$ at which the atmosphere of carbon atoms can follow a moving screw dislocation.
- Self consistent calculation of average velocity of screw dislocation in binary iron–carbon alloys gliding by a high-temperature kink-pair mechanism under constant strain rate.

We conduct a quantitative analysis of the conditions of stress and temperature at which screw dislocation glide is accomplished by a high-temperature kink-pair mechanism. We conclude that several factors are responsible for the viscous dislocation glide observed above about 200 °C in iron—carbon alloy:

- At high temperatures, kink-pair formation enthalpy E_{kp} decreases as a consequence of the increased carbon mobility in the dislocation core and reduced number of segregated C atoms.
- The enhanced diffusivity of carbon both in the core region and in dislocation surroundings lead to higher maximal dislocation velocity $v_{\max}$ at which the atmosphere of carbon atoms can follow a moving screw dislocation.

In accordance with the experimental observations, the present simulations reveal that at high temperatures (T = 500 K), 1/2[111] screw dislocation glide in iron–carbon alloy is accomplished by a high-temperature kink-pair mechanism. At intermediate temperatures (T = 400 K), thermally-activated smooth dislocation propagation is interrupted by sporadic bursts of screw dislocation activity.

Author Contributions: Conceptualization, I.H.K. and L.B.D. All authors have read and agreed to the published version of the manuscript.

Funding: This research was funded in part by the Bulgarian Science Fund under the National Scientific Program "Petar Beron i NIE" (Project UMeLaMP), UKRI Grant EP/V001787/1 and by the European Regional Development Fund, within the Operational Programme "Science and Education for Smart Growth 2014–2020" under the Project CoE "National centre of mechatronics and clean technologies" BG05M20P001-1.001-0008-C01.

Institutional Review Board Statement: Not applicable.

Informed Consent Statement: Not applicable.

Data Availability Statement: Not applicable.

Conflicts of Interest: The authors declare no conflict of interest.

References

1. Caillard, D. An in situ study of hardening and softening of iron by carbon interstitials. *Acta Mater.* **2011**, *59*, 4974–4989. [CrossRef]
2. Cottrell, A.H.; Bilby, B.A. Dislocation theory of yielding and strain ageing of iron. *Proc. Phys. Soc. Sect. A* **1949**, *62*, 49–62. [CrossRef]
3. Clouet, E.; Garruchet, S.; Nguyen, H.; Perez, M.; Becquart, C.S. Dislocation interaction with C in α-Fe: A comparison between atomic simulations and elasticity theory. *Acta Mater.* **2008**, *56*, 3450–3460. [CrossRef]
4. Li, Y.; Choi, P.; Borchers, C.; Westerkamp, S.; Goto, S.; Raabe, D.; Kirchheim, R. Atomic-scale mechanisms of deformation-induced cementite decomposition in pearlite. *Acta Mater.* **2011**, *59*, 3965–3977. [CrossRef]
5. Allera, A.; Ribeiro, F.; Perez, M.; Rodney, D. Carbon-induced strengthening of bcc iron at the atomic scale. *Phys. Rev. Mater.* **2022**, *6*, 013608. [CrossRef]
6. Patinet, S.; Bonamy, D.; Proville, L. Atomic-scale avalanche along a dislocation in a random alloy. *Phys. Rev. B* **2011**, *84*, 174101. [CrossRef]
7. Zhao, Y.; Dezerald, L.; Pozuelo, M.; Zhou, X.; Marian, J. Simulating the mechanisms of serrated flow in interstitial alloys with atomic resolution over diffusive timescales. *Nat. Commun.* **2020**, *11*, 1–8. [CrossRef] [PubMed]
8. Zhao, Y.; Marian, J. Direct prediction of the solute softening -to-hardening transition in W-Re alloys using stochastic simulations of screw dislocation motion. *Model. Simul. Mater. Eng.* **2018**, *26*, 045002. [CrossRef]
9. Caillard, D. Dynamic strain ageing in iron alloys: The shielding effect of carbon. *Acta Mater.* **2016**, *112*, 273–284. [CrossRef]
10. Katzarov, I.H.; Drenchev, L.B.; Pashov, D.L.; Zarrouk, T.N.A.T.; Al-lahham, O.; Paxton, A.T. Dynamic strain aging and the rôle Dynamic strain aging and the rôle of the Cottrell atmosphere. 2022, *submitted*.
11. Nematollahi, G.A.; Grabowski, B.; Raabe, D.; Neugebauer, J. Multiscale description of carbon-supersaturated ferrite in severely drawn pearlitic wires. *Acta Mater.* **2016**, *111*, 321–334. [CrossRef]
12. Wilde, J.; Cerezo, A.; Smith, G.D.W. Three-dimensional atomic-scale mapping of a Cottrell atmosphere around a dislocation in iron. *Scr. Mater.* **2000**, *43*, 39–48. [CrossRef]
13. Gong, P.; Katzarov, I.H.; Nutter, J.; Paxton, A.T.; Rainforth, W.M. The influence of hydrogen on plasticity in pure iron–theory and experiment. *Sci. Rep.* **2020**, *10*, 10209. [CrossRef] [PubMed]
14. Katzarov, I.H.; Pashov, D.L.; Paxton, A.T. Hydrogen embrittlement I. Analysis of hydrogen-enhanced localized plasticity: Effect of hydrogen on the velocity of screw dislocations in α-Fe. *Phys. Rev. Mater.* **2017**, *1*, 033602. [CrossRef]
15. Itakura, M.; Kaburaki, H.; Yamaguchi, M.; Okita, T. The Effect of Hydrogen Atoms on the Screw Dislocation Mobility in Bcc Iron: A First-Principles Study. *Acta Mater.* **2013**, *61*, 18. [CrossRef]
16. Clouet, E.; Ventelon, L.; Willaime, F. Dislocation core energies and core fields from first principles. *Phys. Rev. Lett.* **2009**, *102*, 055502. [CrossRef] [PubMed]
17. Zarrouk, T. Atomistic Investigation of Dislocation-Assisted Carbon Migration in Iron. Ph.D. Thesis, King's College London, London, UK, 2022.
18. Paxton, A.T.; Elsässer, C. Analysis of a Carbon Dimer Bound to a Vacancy in Iron Using Density Functional Theory and a Tight Binding Model. *Phys. Rev. B* **2012**, *87*, 22. [CrossRef]
19. Ventelon, L.; Lüthi, B.; Clouet, E.; Proville, L.; Legrand, B.; Rodney, D.; Willaime, F. Dislocation core reconstruction induced by carbon segregation in bcc iron. *Phys. Rev. B* **2015**, *91*, 220102(R). [CrossRef]
20. Hirth, J.P.; Lothe, J. *Theory of Dislocations*, 1st ed.; McGraw-Hil Book Company: New York, NY, USA, 1968.

21. Henkelman, G.; Jónsson, H. Improved tangent estimate in the nudged elastic band method for finding minimum energy paths and saddle points. *J. Chem. Phys.* **2000**, *113*, 9978–9985. [CrossRef]
22. Itakura, M.; Kaburaki, H.; Yamaguchi, M. First-principles study on the mobility of screw dislocations in bcc iron. *Acta Mater.* **2012**, *60*, 3698–3710. [CrossRef]